Communication

CoCrFeNi Multi-principal Element Alloy Prepared *Via* Self-propagating High-Temperature Synthesis Plus Investment Casting Method

TAO LU, WENKE CHAI, YE PAN, TING DAI, and DONGKE SUN

A CoCrFeNi multi-principal element alloy was successfully prepared *via* the combination of self-propagating high-temperature synthesis and investment casting. The phase identification, the as-cast microstructure, and the solidification phenomena were investigated. Unlike the dendrite morphology obtained by arc melting, cellular growth in the as-cast alloy was observed as a consequence of the rapid solidification. The solidification process is discussed with regard to the rate of advance of the liquid–solid interface, the equilibrium melting range, and the interface temperature gradient.

https://doi.org/10.1007/s11663-018-1477-3
© The Minerals, Metals & Materials Society and ASM International 2018

INTRODUCTION

Multi-principal element alloys (MPEAs), also known as high-entropy alloys, have been considered a discrete category of metallic materials since their discovery in 2004.[1] Distinguishing them from conventional alloys, which have one or two elements as the principal components, the design of MPEAs extends the number of principal elements up to four or five, and the concentrations of each element are almost equal. An MPEA can usually be characterized by a single-phase solid solution, such as those with structures of face-centered cubic (FCC) (CoCrFeMnNi[2]), body-centered cubic (NbMoTaW[3]), and hexagonal close packing (DyGdLuTbY[4]). With microalloying and alteration of the composition ratio, the structure may present with dual solid-solution phases (*e.g.*, high-entropy eutectic alloys[5,6]) or a single-phase solid solution containing a small quantity of intermetallics. Nevertheless, the number of phases in an MPEA are much fewer than predicted by the phase law.[7–9] This phenomenon can be attributed to the 'high-entropy effect,' where the higher configurational entropy, induced by five or more elements in a near-equimolar alloy, favors the formation of solid-solution phases instead of intermetallic compounds.[10] Furthermore, the main characteristics in an MPEA, such as high-entropy, sluggish diffusion, severe lattice distortion, and the cocktail effect, have led to the modification of traditional physical metallurgy principles that were mainly constructed based on investigations of conventional alloys.[11]

To date, over 400 distinct MPEAs have been reported[12]; however, their preparation type can be classified into only four methods. The first is that of arc or induced melting in a vacuum, followed by thermomechanical processing of the ingots combined with annealing to obtain fully recrystallized grains.[13–15] The second method involves mechanical alloying followed by hot isostatic pressing or spark plasma sintering to obtain nano- or ultrafine-grained MPEAs.[16–18] The third method employs laser cladding or magnetron sputtering to produce MPEA coatings on different substrates.[19–21] The fourth approach is that of additive manufacturing, which employs selective laser melting and electron beam melting technologies.[22–24] In addition, Sanin *et al.*[25] reported in 2016 that a CrCoFeMnNiAl$_x$ MPEA system was prepared by self-propagating high-temperature synthesis (SHS) using a centrifugal arrangement. With different contents of Al, the composition varied from a single FCC phase to a complex structure comprising FCC, BCC, and β-NiAl. This result indicated that SHS is an alternative and promising technology to prepare MPEAs, having advantages of high purity of products and cost efficiency. In this study, we report precision shaping of a CoCrFeNi MPEA *via* SHS combined with investment casting under atmospheric conditions. This alloy is quite ductile and may be processed by thermomechanical processing to improve its microstructure and properties. The microstructure, phase identification, and solidification behavior of the as-cast MPEA were systematically investigated. The results of this study may extend the development of shape casting of MPEAs.

The synthesis of the CoCrFeNi MPEA is based on the thermite reaction between Al and the metal oxides of Co_2O_3, Cr_2O_3, Fe_2O_3, and NiO in a stoichiometric ratio. Analytical-grade reactant powders were supplied by Sinopharm Chemical Reagent Co., Ltd. (PR China) and had an average particle size of 75 μm. The powders were mixed in a planetary ball mixer at 300 r/min for 4 hours, using alcohol as the process control agent. Steel vials

TAO LU, WENKE CHAI, YE PAN, and TING DAI are with the School of Materials Science and Engineering, Jiangsu Key Laboratory of Advanced Metallic Materials, Southeast University, Nanjing 211189, China. Contact e-mail: panye@seu.edu.cn DONGKE SUN is with the Jiangsu Key Laboratory for Design and Manufacture of Micro-Nano Biomedical Instruments, School of Mechanical Engineering, Southeast University, Nanjing 211189, China.

Manuscript submitted March 24, 2018.
Article published online December 10, 2018.

and balls were used, and the ball-to-powder mass ratio was 4:1. After drying in a vacuum oven, 30 g of the powder mixture was pressed into a 20-mm-diameter cylinder steel mold to obtain a green compact with 60 pct theoretical maximum density.

Preparation of the investment mold comprised the following steps: (1) a wax model (diameter: 4 mm; height: 20 mm) was prepared and assembled within a graphite mold; (2) a degassed gypsum casting slurry was poured into the steel cylinder and hardened at room temperature; (3) the mold was dewaxed and baked in an electric oven, upon heating at 150 °C for 2 hours, at 350 °C for 3 hours, and then at 750 °C for 3 hours; and (4) the mold was furnace cooled to 300 °C prior to casting of the MPEA.

Figure 1(a) shows a schematic of the self-designed device for the synthesis and casting process. The green compact was placed into the graphite crucible to prevent damage to the gypsum mold, because the reaction temperature may exceed 2000 °C. A Ni-Cr heating wire was used as the ignitor to rapidly heat the surface of the compact. The self-sustained thermite reaction can be ignited in approximately 5 seconds. After the reaction was completed, the MPEA melt was separated from the Al_2O_3 product based on the difference in their densities and was cast into the graphite mold by subjecting the investment mold under vacuum. Figures 1(b) and (c) present photographs of the as-cast MPEA rods.

For metallographic observation and phase identification, each sample was sectioned from an as-cast rod and polished to a fine finish (2.5 μm diamond suspension), then etched in a solution of HF:HNO_3 = 1:3 for 15 seconds. The microstructure was characterized by optical microscopy (Olympus BX-60M, Japan) and scanning electron microscopy (FEI Sirion) coupled with energy-dispersive spectroscopy (EDS) and electron backscattered diffraction (EBSD). Phase identification was carried out by X-ray diffraction (XRD; D8-Discover, Bruker, Germany) using Cu-K_α radiation (λ = 0.154 nm).

Figure 2(a) shows an XRD pattern of an as-cast MPEA specimen. Four characteristic peaks are evident, which were indexed to the (1, 1, 1), (2, 0, 0), (2, 2, 0), and (3, 1, 1) planes of the FCC phase. Within the accuracy limits of the technique, no other peaks were detected, suggesting that only a single solid-solution FCC phase with a lattice constant of a $\approx$ 0.357 nm existed in the sample. The microstructure, shown in Figure 2(b), presented a uniformly distributed cellular structure, but the grain size is in the range of 100 to 500 μm determined by the distance away from the surface of the ingot according to EBSD results, shown in Figure 3(a). The average size of each cell was about 2 to 3 μm, and the width of the intercellular space was approximately 0.5 μm (Figure 3(b)). EDS mapping of the principal elements indicated no obvious compositional segregation, and the distribution of the individual elements was homogeneous throughout the sample.

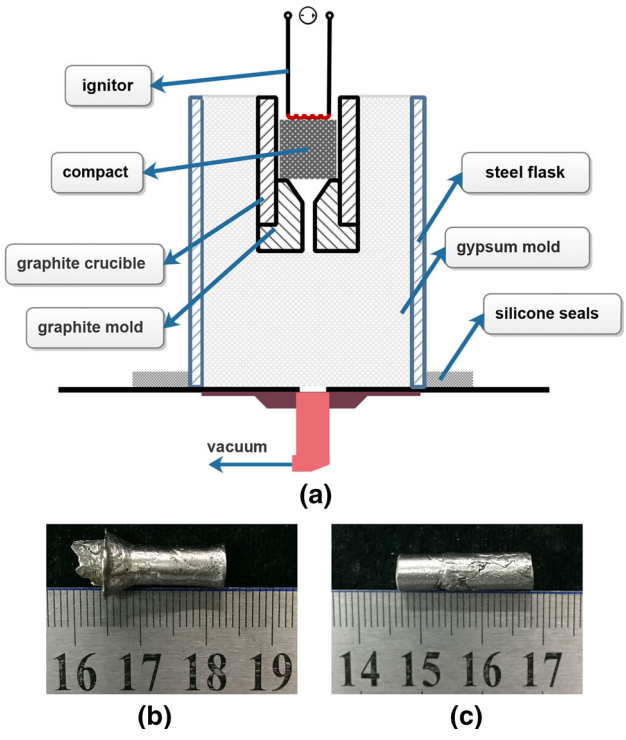

Fig. 1—(*a*) Schematic of device employed for preparation of multi-principal element alloy employing self-propagating high-temperature synthesis with investment casting. (*b*, *c*) Photographs of as-cast alloys.

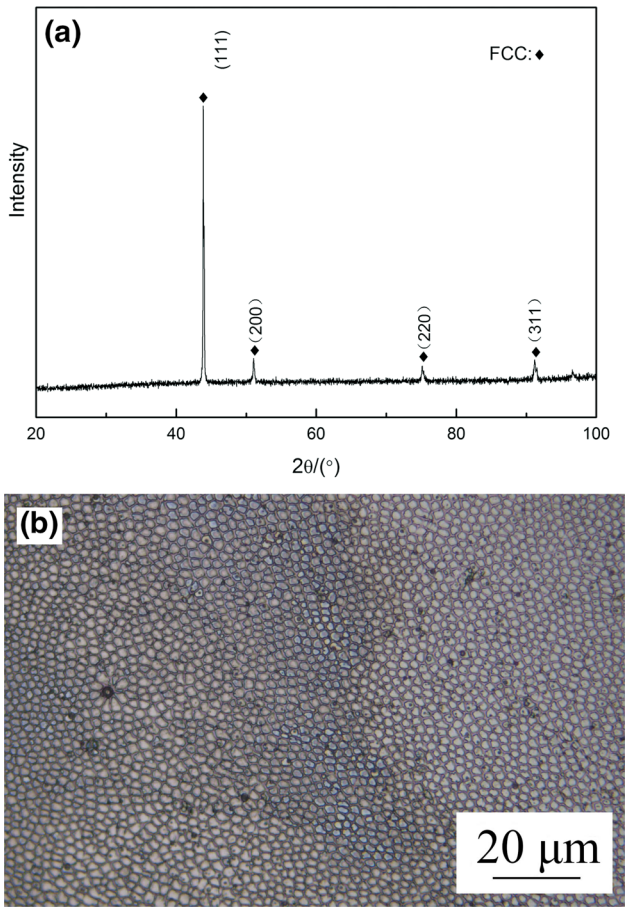

Fig. 2—(*a*) X-ray diffraction showing a single face-centered cubic phase. (*b*) Optical micrograph exhibits cellular morphology of etched sample.

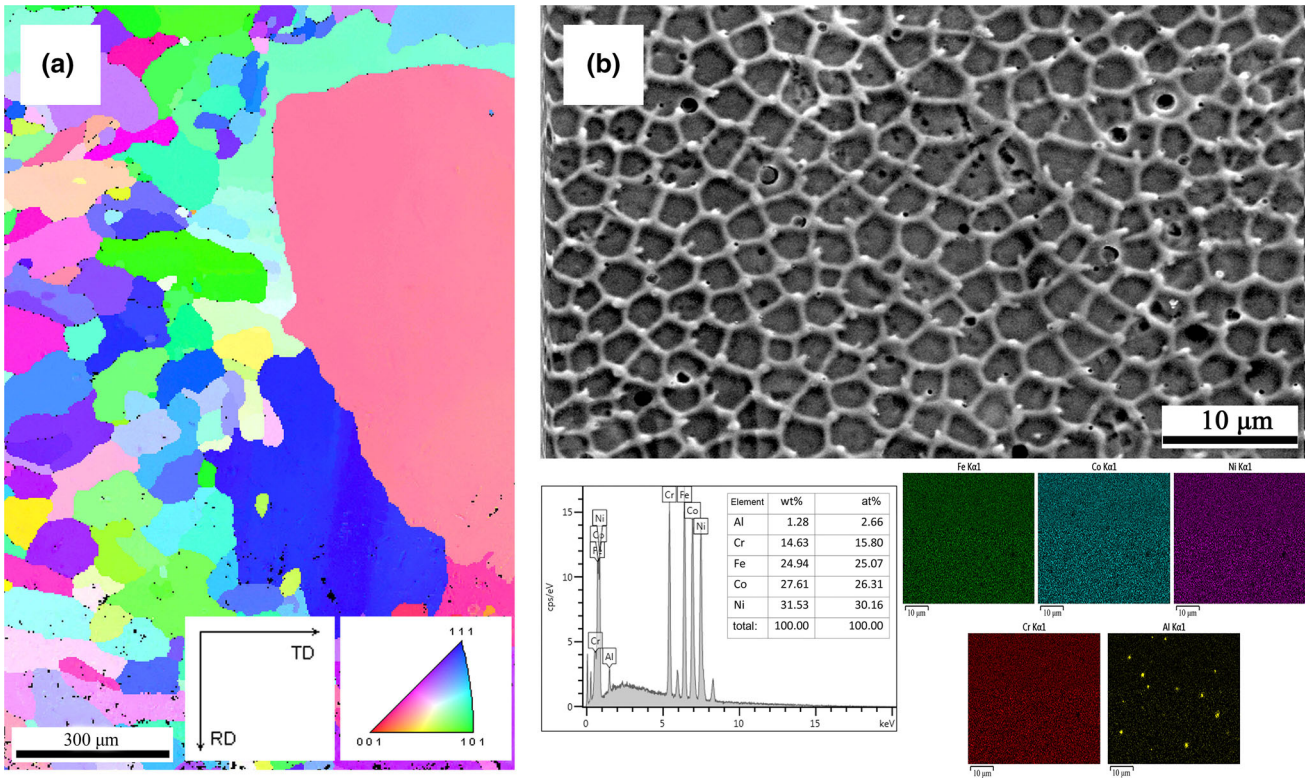

Fig. 3—(*a*) Electron backscattered diffraction result with the grain size being much larger than the cells observed by optical or (*b*) scanning electron microscopy. Energy-dispersive spectral maps below indicate the homogeneous size and elemental distribution of the cells. No obvious elemental segregation is observed.

It is worth noting that the content of Cr (~ 15 at. pct) was less than the designed composition, and trace alloying of Al (~ 2 at. pct) existed in the matrix. This is because the rapid combustion process may lead to a locally incomplete reaction within the green compact; therefore, a trace amount of unreacted Al can be trapped in the matrix by the high-temperature melt. Alternatively, the reaction enthalpy at 25 °C of Al-Cr_2O_3 (− 540.991 kJ) is much less negative than those of Al-Fe_2O_3 (− 852.692 kJ), Al-NiO (− 956.592 kJ), and Al-CoO (− 961.860 kJ) (all values calculated employing *HSC Chemistry* software (Outotec, Finland)), so it is more difficult to produce Cr than the other metallic elements by the thermite reaction. Consequently, the Al-Cr_2O_3 reaction may not proceed to completion.

The cellular structure formed in the experimental alloy differs considerably when compared with reported CoCrFeNi high-entropy alloys prepared *via* arc melting, in which the structure usually shows dendritic morphology. The homogeneous distribution of smaller cells implies a much higher migration velocity of the liquid–solid interface during solidification and is similar to the structure obtained in the laser melting of high-concentration alloys, such as 316L stainless steel[26] and nickel-based alloys.[27] The fast rate of solidification of the liquid–solid interface is attributed to quenching of the MPEA melt produced by the SHS reaction from a much higher temperature (normally up to 2000 °C).

Figure 4 presents the phase diagrams of CoFeNi and CoCrFeNi MPEA alloys, as determined by means of *Pandat* software (CompuTherm). The equilibrium melting range of the CoFeNi alloy is very small, 0.25 K, but the presence of Cr enlarges the melting range to 20 to 30 K. The morphological instability of the liquid–solid interface can be expressed as follows[28]:

$$\frac{G}{V} \leq \frac{\Delta T_0}{D}, \qquad [1]$$

where G is the interface temperature gradient, V is the rate of interface movement, ΔT_0 is the equilibrium melting range, and D is the diffusion coefficient in the liquid. The liquid–solid interface will be unstable because Eq. [1] is satisfied. It is evident that a small value of ΔT_0 is beneficial to stabilization of the liquid–solid interface to suppress cellular or dendrite growth. The addition of Cr increases the constitutional undercooling, which promotes instability of the interface, so cellular growth can also be preferred under the higher G of rapid solidification.

In this study, we presented a preparation strategy for CoCrFeNi MPEA employing the combination of SHS and investment casting. This strategy can be further extended to other MPEA alloys in which the principal elements can be produced by the thermite reaction. The fine cellular structure obtained in the as-cast ingot can be attributed to rapid solidification of the liquid–solid interface. The addition of Cr increased the constitutional undercooling of CoCrFeNi MPEA, which

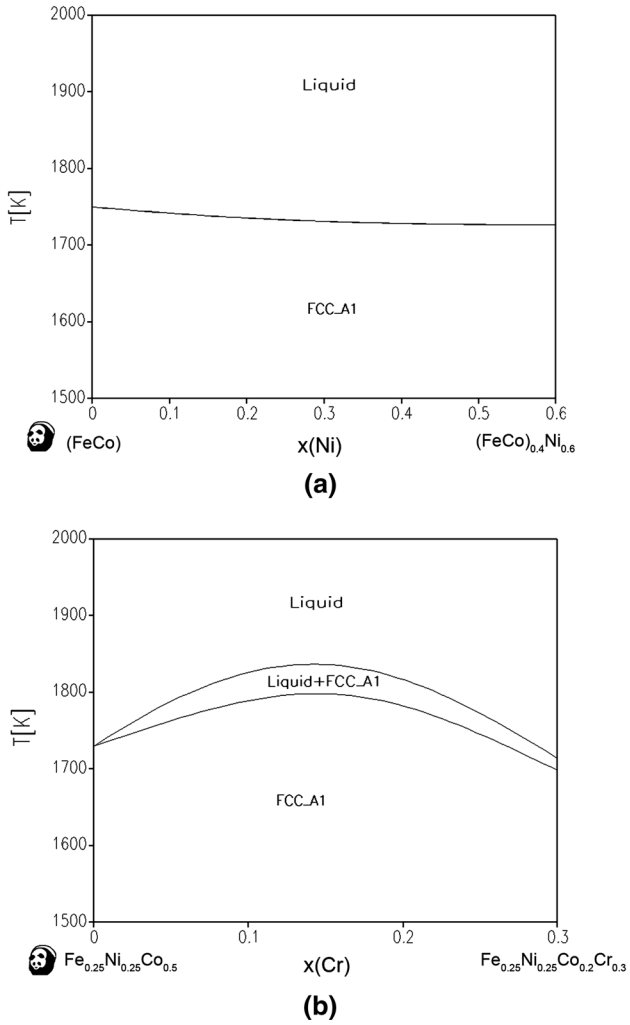

Fig. 4—Isopleths along (*a*) (FeCo)-Ni in FeCoNi alloy and (*b*) Co-Cr in CoCrFeNi alloy.

promoted instability of the interface, but cellular growth was preferred under the higher G of rapid solidification.

This study was supported by the National Natural Science Foundation of China (Grant Nos. 51671056 and 51728601) and Jiangsu Key Laboratory for Advanced Metallic Materials (Grant No. BM2007204). We thank Kathryn Sole, Ph.D., from Liwen Bianji, Edanz Group China (www.liwenbianji.cn/ac), for editing the English text of the earlier draft of this manuscript.

REFERENCES

1. J.W. Yeh, S.K. Chen, S.J. Lin, J.Y. Gan, T.S. Chin, T.T. Shun, C.H. Tsau, and S.Y. Chang: *Adv. Eng. Mater.*, 2004, vol. 6, pp. 299–303.
2. B. Gludovatz, A. Hohenwarter, D. Catoor, E.H. Chang, E.P. George, and R.O. Ritchie: *Science*, 2014, vol. 345, pp. 1153–58.
3. O.N. Senkov, G.B. Wilks, D.B. Miracle, C.P. Chuang, and P.K. Liaw: *Intermetallics*, 2010, vol. 18, pp. 1758–65.
4. A. Takeuchi, K. Amiya, T. Wada, K. Yubuta, and W. Zhang: *Jom*, 2014, vol. 66, pp. 1984–92.
5. X.Z. Gao, Y.P. Lu, B. Zhang, N.N. Liang, G.Z. Wu, G. Sha, J.Z. Liu, and Y.H. Zhao: *Acta Mater.*, 2017, vol. 141, pp. 59–66.
6. H. Jiang, K.M. Han, X.X. Gao, Y.P. Lu, Z.Q. Cao, M.C. Gao, J.A. Hawk, and T.J. Li: *Mater. Des.*, 2018, vol. 142, pp. 101–05.
7. J.Y. He, W.H. Liu, H. Wang, Y. Wu, X.J. Liu, T.G. Nieh, and Z.P. Lu: *Acta Mater.*, 2014, vol. 62, pp. 105–13.
8. W.H. Liu, Z.P. Lu, J.Y. He, J.H. Luan, Z.J. Wang, B. Liu, Y. Liu, M.W. Chen, and C.T. Liu: *Acta Mater.*, 2016, vol. 116, pp. 332–42.
9. T.T. Zuo, M.C. Gao, L.Z. Ouyang, X. Yang, Y.Q. Cheng, R. Feng, S.Y. Chen, P.K. Liaw, J.A. Hawk, and Y. Zhang: *Acta Mater.*, 2017, vol. 130, pp. 10–18.
10. Y. Zhang, J.W. Yeh, J.F. Sun, J.P. Lin, and K.F. Yao: *Adv. Mater. Sci. Eng.*, 2015, vol. 2015, pp. 1–1.
11. J.W. Yeh: *Jom*, 2015, vol. 67, pp. 2254–61.
12. D.B. Miracle and O.N. Senkov: *Acta Mater.*, 2017, vol. 122, pp. 448–511.
13. Y. Deng, C.C. Tasan, K.G. Pradeep, H. Springer, A. Kostka, and D. Raabe: *Acta Mater.*, 2015, vol. 94, pp. 124–33.
14. Z.Y. Liu, S. Guo, X.J. Liu, J.C. Ye, Y. Yang, X.L. Wang, L. Yang, K. An, and C.T. Liu: *Scr. Mater.*, 2011, vol. 64, pp. 868–71.
15. B. Vishwanadh, N. Sarkar, S. Gangil, S. Singh, R. Tewari, G.K. Dey, and S. Banerjee: *Scr. Mater.*, 2016, vol. 124, pp. 146–50.
16. Z.Q. Fu, W.P. Chen, H.M. Wen, D.L. Zhang, Z. Chen, B.L. Zheng, Y.Z. Zhou, and E.J. Lavernia: *Acta Mater.*, 2016, vol. 107, pp. 59–71.
17. C. Wang, W. Ji, and Z.Y. Fu: *Adv. Powder Technol.*, 2014, vol. 25, pp. 1334–38.
18. S. Varalakshmi, G.A. Rao, M. Kamaraj, and B.S. Murty: *J. Mater. Sci.*, 2010, vol. 45, pp. 5158–63.
19. C.F. Tsai, P.W. Wu, P. Lin, C.G. Chao, and K.Y. Yeh: *Japanese Journal of Applied Physics*, 2008, vol. 47, pp. 5755–61.
20. C. Huang, Y.Z. Zhang, R. Vilar, and J.Y. Shen: *Mater. Des.*, 2012, vol. 41, pp. 338–43.
21. H. Zhang, Y.Z. He, and Y. Pan: *Scr. Mater.*, 2013, vol. 69, pp. 342–45.
22. V. Ocelik, N. Janssen, S.N. Smith, and J.T.M. De Hosson: *Jom*, 2016, vol. 68, pp. 1810–18.
23. Y. Brif, M. Thomas, and I. Todd: *Scr. Mater.*, 2015, vol. 99, pp. 93–96.
24. J. Joseph, N. Stanford, P. Hodgson, and D.M. Fabijanic: *Scripta Mater.*, 2017, vol. 129, pp. 30–34.
25. V.N. Sanin, V.I. Yukhvid, D.M. Ikornikov, D.E. Andreev, N.V. Sachkova, and M.I. Alymov: *Dokl. Phys. Chem.*, 2016, vol. 470, pp. 145–49.
26. W.Y. Huo, H. Zhou, F. Fang, Z.H. Xie, and J.Q. Jiang: *Mater. Des.*, 2017, vol. 134, pp. 226–33.
27. P. Sathiyamoorthi, J. Basu, S. Kashyap, K.G. Pradeep, and R.S. Kottada: *Mater. Des.*, 2017, vol. 134, pp. 426–33.
28. X.Q. Zhou, H. Zhong, D.D. Yu, Z.C. Wen, W.B. Cui, and Q. Wang: *J. Magn. Magn. Mater.*, 2017, vol. 442, pp. 67–71.